

Article

Facile Synthesis of a Broad Range of Colloidal Nanocrystals by Membrane-Mediated pH Gradient under Ambient Conditions

Shahab Ranjbar Bahadori¹, Ryan Hart¹, Aditi Mulgaonkar², Yunfeng Wang³, Samuel Fuentes¹, Yi Hong⁴ , Ye Cao¹, Jiechao Jiang^{1,*} , Xiankai Sun^{2,*}  and Yaowu Hao^{1,*}

¹ Department of Materials Science and Engineering, University of Texas at Arlington, Arlington, TX 76019, USA; shahab.ranjbarbahadori@mavs.uta.edu (S.R.B.); ryan.hart@mavs.uta.edu (R.H.); samuel.fuentes2@mavs.uta.edu (S.F.); ye.cao@uta.edu (Y.C.)

² Department of Radiology, University of Texas Southwestern Medical Center, Dallas, TX 75390, USA; aditi.mulgaonkar@utsouthwestern.edu

³ Department of Mechanical Engineering, The College of New Jersey, Ewing, NJ 08618, USA; jwang@tcnj.edu

⁴ Department of Bioengineering, University of Texas at Arlington, Arlington, TX 76019, USA; yihong@uta.edu

* Correspondence: jiangjc@uta.edu (J.J.); xiankai.sun@utsouthwestern.edu (X.S.); yhao@uta.edu (Y.H.)

Abstract: We report a simple synthesis process for a wide variety of ultrasmall nanocrystals. Simply immersing a dialysis bag containing an aqueous solution of a metal salt mixed with citric acid in a NaOH solution reservoir for 10 min, nanocrystals measuring only a few nanometers in size are formed inside the dialysis bag. We demonstrated the synthesis of ultrasmall nanocrystals of Co, Ni, Cu, Ag, Au, Pd, Cu₂O, FeO, and CeO₂, and found that the gradual change in pH caused by the diffusion of OH[−] ions through the dialysis membrane played an essential role in the formation of these nanocrystals. This method can be readily adapted for almost all transition metal elements, providing researchers in the fields of catalysis and nanomedicine an easy access to a wide range of ultrasmall metal and oxide nanocrystals.

Keywords: nanocrystals; nanoparticle synthesis; liquid diffusion



Citation: Ranjbar Bahadori, S.; Hart, R.; Mulgaonkar, A.; Wang, Y.; Fuentes, S.; Hong, Y.; Cao, Y.; Jiang, J.; Sun, X.; Hao, Y. Facile Synthesis of a Broad Range of Colloidal Nanocrystals by Membrane-Mediated pH Gradient under Ambient Conditions. *Crystals* **2024**, *14*, 240. <https://doi.org/10.3390/cryst14030240>

Academic Editor: Jaime Gómez Morales

Received: 28 January 2024

Revised: 25 February 2024

Accepted: 27 February 2024

Published: 29 February 2024



Copyright: © 2024 by the authors. Licensee MDPI, Basel, Switzerland. This article is an open access article distributed under the terms and conditions of the Creative Commons Attribution (CC BY) license (<https://creativecommons.org/licenses/by/4.0/>).

1. Introduction

The last two decades have seen an exponential growth in research into the synthesis of colloidal metal and metal oxide nanocrystals, which is one of the most active research fields in chemistry. This was initially driven by the potential usage of colloidal nanocrystals as a building block for heterogeneous catalysts for chemical industry and as a model system to study their catalytic mechanisms [1,2]. Later, their potential applications as nanomedicine [3,4] and artificial enzymes (nanozymes) [5,6] further fueled enthusiasm in this research field.

Myriad methods have been developed and optimized to synthesize a variety of nanocrystals [7,8]. For metal nanocrystals, there are, in general, two strategies [7,8]: bottom-up and top-down methods. In the bottom-up approach, metal nanocrystals are synthesized by reducing metal ion precursors in the presence of suitable ligands. It is the most efficient way to nucleate clusters (nanocrystals), and most importantly, such nucleation can be controlled by varying the quantities of the ligands and reducing agents or by varying the solvents. Aqueous and organic soluble metal nanocrystals can be produced using these wet chemical methods [9] such as the reduction in metal salts [10–16] and the decomposition of organometallic precursors [17–20]. Though this approach is the most popular synthesis method for metal nanocrystals, such synthesis is usually conducted at an elevated temperature, and often uses an expensive or dangerous reducing agent such as inorganic or organic hydrides and organic solvent. To speed up the chemical reactions, different energy forms have been applied to assist the nanocrystal synthesis process. Microwave irradiation has

been used for the synthesis of uniform and monodisperse Au nanocrystals [21]. Electromagnetic field of microwave causes the oscillating friction between polarized molecules, which heat up the entire solution. Homogeneous and rapid heating in a solution induced by the microwave irradiation can offer homogeneous nucleation and shorter crystallization times. Sonochemical synthesis is another effective strategy for preparing nanocrystals, in which ultrasound is irradiated into a liquid and triggers the nucleation, growth, and implosive collapse of bubbles (acoustic cavitation) in liquid [22]. During treatment, very high temperature, pressure, and extremely rapid cooling rates can be achieved, so providing a unique platform for the growth of nanocrystals [23,24]. In 2001, Dickson et al. [25] first demonstrated that nanocrystals could be produced by photoreduction without the addition of reduction agents. Metal ions encapsulated in microgel could efficiently and spontaneously form nanoclusters under sunlight. Aqueous microgel dispersions can produce H^\bullet , OH^\bullet , and perhaps also other organic radicals by the irradiation of UV, which can reduce metal ions into metal atoms [26]. In the top-down method, a metal nanoparticle is initially synthesized which is then treated with extra ligands or metal ions to form nanocrystals [27–34]. In such ligand-induced etching, atoms are detached from the nanoparticles surface by the ligand and then form nanoclusters through strong atom–atom interactions [35]. For the case of gold nanocrystals, in the presence of excess thiol, the surface-Au atoms of AuNPs are removed leading to the formation of Au(I)-thiolate complexes and these complexes can then undergo strong Au(I)–Au(I) interactions to form gold nanoclusters [36].

For metal oxide nanocrystals, the focus has been on the superparamagnetic iron oxide (magnetite Fe_3O_4 or maghemite Fe_2O_3) nanocrystals (SPIONs). In the last three decades, mainly driven by their potential biomedical applications such as serving as MRI contrast and/or hyperthermia treatment agents, many synthesis methods have been developed to produce SPIONs, including co-precipitation [37,38], hydrothermal and solvothermal syntheses [39–42], thermal decomposition [43,44], microemulsion [45], sol-gel reaction and polyol [46,47], sonochemical [48], and microwave-assisted synthesis [49]. But co-precipitation and hydrothermal and solvothermal syntheses are by far the most commonly used method. Using the co-precipitation method to produce magnetite nanoparticles is a convenient and low-cost method enabling rapid, large-scale production, in which salts of Fe^{2+} and Fe^{3+} ions (with molar ratio 1:2) co-precipitate in a basic solution at room temperature or under heat. However, the resulting nanoparticles have a fairly large size distribution and often aggregate together with a poor crystallinity which may compromise their magnetic properties. Hydrothermal and solvothermal syntheses typically create SPIONs with an excellent uniformity. In the hydrothermal method, iron precursors are exposed to vapor in a sealed container and placed under high pressure and temperature conditions in an aqueous medium. The solvothermal method replaces water by other organic solvents, allowing the formation of monodisperse SPIONs with higher crystallinity and better controlled shapes. But SPIONs synthesized with organic solvent are usually hydrophobic and often need a ligand exchange process to be transferred into water.

Here, we report a simple process using aqueous solution at room temperature to produce a variety of ultrasmall metal and metal oxide nanocrystals. In this method, no particular setup is needed; only a beaker and a piece of dialysis membrane are used. Dialysis membrane is commonly used in biology laboratories for a variety of applications including desalting, buffer exchange, removal of labeling reagents, drug binding studies, cell growth and feeding, virus purification, and blood treatment. Dialysis membranes are composed of regenerated cellulose and contain a broad range of pore sizes to separate molecules based on size. This is the first time that dialysis tubes have been used in nanocrystal synthesis. We make use of the gradual change in pH caused by the diffusion of OH^- ions through the dialysis membrane to simultaneously access a wide range of pH in the solution, including a pH that can trigger a chemical reaction to produce nanoparticles. This simple method can be readily adapted for almost all transition metal elements. Therefore, it can provide researchers in different fields an easy access to a wide range of ultrasmall metal and oxide nanocrystals, which is particularly useful for scientists without a regular wet chemistry lab.

2. Materials and Methods

2.1. Materials

The chemicals including cobalt (II) chloride hexahydrate ($\text{CoCl}_2 \cdot 6\text{H}_2\text{O}$, 98%), nickel (II) chloride hexahydrate ($\text{NiCl}_2 \cdot 6\text{H}_2\text{O}$, 98%), copper(II) chloride dihydrate ($\text{CuCl}_2 \cdot 2\text{H}_2\text{O} \geq 99.0\%$), silver nitrate (AgNO_3 , 99%), gold (III) chloride trihydrate ($\text{HAuCl}_4 \cdot 3\text{H}_2\text{O}$, 99.9%), platinum (II) chloride (PtCl_2 , 98%), palladium (II) chloride (PdCl_2 , 99%), cerium (II) chloride heptahydrate ($\text{CeCl}_2 \cdot 7\text{H}_2\text{O}$, 99.9%), citric acid ($\text{C}_6\text{H}_8\text{O}_7$, 99.5%), and dialysis tubing cellulose membrane (MWCO 14000) were purchased from Sigma-Aldrich (St. Louis, MO, USA). Furthermore, copper (II) chloride dihydrate ($\text{CuCl}_2 \cdot 2\text{H}_2\text{O}$, 99%) was obtained from Alfa Aesar (Ward Hill, MA, USA) and sodium hydroxide (NaOH , 97%) was purchased from Thermo Fisher Scientific (Waltham, MA, USA). All aqueous solutions were prepared in Millipore Milli-Q DI water (18 M Ω cm) which was provided from a Millipore Gradient Milli-Q water system (Billerica, MA, USA).

2.2. Synthesis Process of Ultrasmall Metallic Nanocrystals

The entire synthesis process for using making metal Cu nanoparticles is illustrated in Figure S1. Simply replacing CuCl_2 with CoCl_2 , NiCl_2 , HAuCl_4 , AgNO_3 , PdCl_2 , and PtCl_2 , respectively, the same process is used to produce Co, Ni, Au, Ag, Pd, and Pt ultrasmall nanoparticles.

First, a mixture of 1.5 mM of citric acid and 1.5 mM of CuCl_2 is stir-mixed for 30 min. Next, the mixture is transferred to a dialysis bag, followed by immersing the dialysis bag into a 0.5 M NaOH solution for 2 h at room temperature. The pH variation was monitored during the synthesis using a Mettler Toledo SevenEasy S20 pH meter (Columbus, OH, USA). At the end of the fixed time period, the solution inside the membrane is collected, followed by centrifugation using an Eppendorf Centrifuge 5418 at 14,000 rpm for about 20 min to precipitate the large precipitates. Then, the resultant supernatant is mixed with acetone at a 4:1 (acetone: supernatant) ratio. The mixture is centrifuged at 14,000 rpm for 20 min. The precipitation is collected and diluted with DI water, and then transferred to a new dialysis bag to be washed inside DI water. For Cu, Ag, Au, Pd, and Pt, the washing process lasted 12 h with DI water being replaced every two hours. For Co and Ni, the washing process lasted 3 h. After washing, the nanoparticle suspension was frozen and lyophilized using a Labconco FreeZone freeze-dryer (Kansas City, MO, USA) to attain the final particle powder.

2.3. Synthesis Process of Ultrasmall Oxide Nanocrystals

While immersing dialysis bag containing copper chloride and citric acid inside NaOH , simultaneous stirring of the solution can develop Cu oxide nanoparticles. First, a mixture of 1.5 mM of citric acid and 1.5 mM of CuCl_2 is stir-mixed for 30 min. Next, the mixture is transferred to a dialysis bag and the dialysis bag is immersed into a 0.05 M NaOH solution for 20 min at room temperature, keeping the solution inside the bag stirring with a magnetic stirring bar placed in a plastic cage. Then, the collected solution is centrifuged at 14,000 rpm for 20 min to separate precipitates of large (several hundred nms) particles. Consequently, the resultant supernatant (with nanocrystals) is mixed with acetone with a 4:1 (acetone:supernatant) ratio and centrifuged at 14,000 rpm for 20 min. Finally, the precipitate is dialysis washed in DI water for about 12 h, while refreshing DI water every 2 h.

2.4. High Resolution Transmission Electron Microscope (HRTEM) and Selected Area Electron Diffraction (SAED)

The HRTEM and SAED were conducted using a Hitachi H-9500 HRTEM operated at an accelerating voltage of 300 kV. The suspension of nanoparticles in DI water was sonicated for about 20 min, and then spread on 300 mesh copper TEM grid covered with a lacey carbon film and dried overnight.

2.5. Magnetic Hysteresis Loop Measurement

The magnetic measurements were conducted at room temperature using a MicroSense EV7 vibrating sample magnetometer (VSM). Ni or Co nanoparticle water suspension (very high concentration) was dropped on a piece of silicon wafer, and then dried. This silicon wafer was measured. The diamagnetic signal from silicon wafer and quartz sample holder was subtracted to obtain ferromagnetic signal from Ni or Co.

2.6. UV-Vis Absorption Measurements

UV-Vis absorbance spectra of Cu, Au, and Ag nanoparticle suspension was measured using a Perkin Elmer Lambda 35 UV-Visible Spectrometer. The samples were prepared by re-suspending the washed metal nanoparticles in about 1.5 mL of DI water, followed by transferring the suspension into 1.5 mL polystyrene semi-micro cuvettes. The slit width was 1 nm and the scanning speed was 120 nm/min.

2.7. Fluorescence Measurements

Fluorescence spectra of colloidal Cu nanoparticles were recorded on a PerkinElmer LS 55 Luminescence Spectrometer using 3.5 mL four-sided fused quartz cuvettes. The slit width was 10 nm and the scanning speed was 100 nm/min.

2.8. Synthesis of Cu Nanocrystals with Different Time

In the same process described above for Cu nanoparticles, the synthesis time (the time of immersion of dialysis bag inside the NaOH reservoir) was varied for 10 min, 20 min, 30 min, 60 min, and 600 min, respectively. The TEM micrographs of resultant Cu nanoparticles are shown in Figure S2.

2.9. Synthesis of Cu Nanocrystals with Varied Concentration of NaOH in the Reservoir

In the same process described above for Cu nanoparticles, the concentration of NaOH in the reservoir was varied for 0.005 M, 0.05 M, 0.1 M. No particles were collected using 0.005 M. The TEM micrographs of resultant Cu nanoparticles using 0.05 M and 0.1 M NaOH are shown in Figure S3.

3. Results

3.1. Metal Nanocrystal Synthesis

Figure 1A depicts our simple setup, in which a dialysis bag containing a metal salt and citric acid mixed in solution is immersed in a NaOH solution reservoir. After the immersion for a certain period, ultrasmall metal or metal oxide nanoparticles form in the solution inside the dialysis bag. We term this method as liquid diffusion synthesis (LDS). Using 1.5 mM respective metal salt and 1.5 mM citric acid in the dialysis bag (10 mL), 0.5 M NaOH in the reservoir (1 L) and an immersion time of 2 h (Figure S1 for details), we obtained ultrasmall nanocrystals of Co, Ni, Cu, Au, Ag, Pd, and Pt (Figures 1B–H and S2). The size of these ultrasmall nanocrystals ranges from 2 nm to 5 nm. Measurements of the magnetic properties of Co and Ni nanoparticles and plasmonic properties of Cu, Au, and Ag nanoparticles confirm that they exist as metallic nanoparticles in solution (not as byproducts of high energy electron beam reduction in HRTEM, since these properties can only result from metal nanocrystals). It should be noted that synthesized Co and Ni nanoparticles are not stable at a pH below 9, dissolving back into ions.

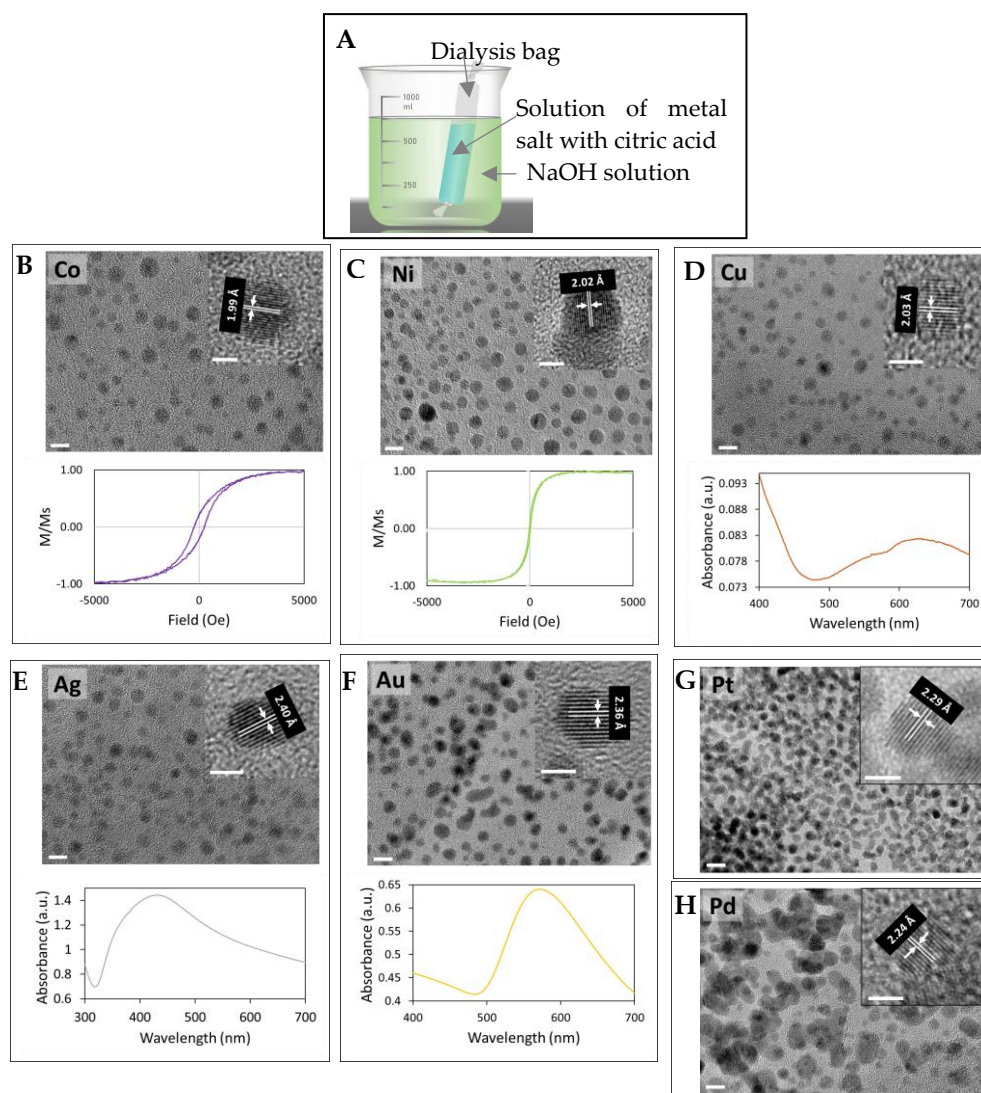


Figure 1. Ultrasmall metal nanocrystals synthesized via LDS. (A) the LDS setup. HRTEM micrographs of Co (B), Ni (C), Cu (D), Ag (E), Au (F), Pt (G), and Pd (H) nanocrystals with magnetic hysteresis loops of Co (B) and Ni (C) nanoparticles and UV-Vis absorption spectra of Cu (D), Au (E) and Ag (F) nanocrystals. The scale bars are 5 nm in TEM micrographs and 2 nm in the insets. All lattice fringes are from (111) planes.

3.2. Cu Nanocrystals

We further chose the LDS process of Cu nanocrystals as a model system for more detailed investigations, aiming to gain an insightful understanding of this method. It was found that the size of nanoparticles is insensitive to the synthesis (immersion) time (Figure S3). This suggests the possibility of upscaling the production of nanocrystals using this method, in which a large dialysis bag is used to hold a large volume of solution which would require a prolonged diffusion process. This process was further optimized by varying NaOH concentration in the reservoir (Figure S4). It was found that using 0.05 M NaOH could produce a large amount of even smaller Cu nanoparticles with a uniform size distribution. Due to their further reduced size ($2\text{ nm} \pm 0.7$, see Figure 2), these nanocrystals become fluorescent with an emission wavelength of 570 nm and an excitation wavelength of 410 nm (Figure 2). This demonstrates that for a particular metal element, the parameters in LDS can be optimized to produce metallic ultrasmall nanoparticles with a narrow size distribution.

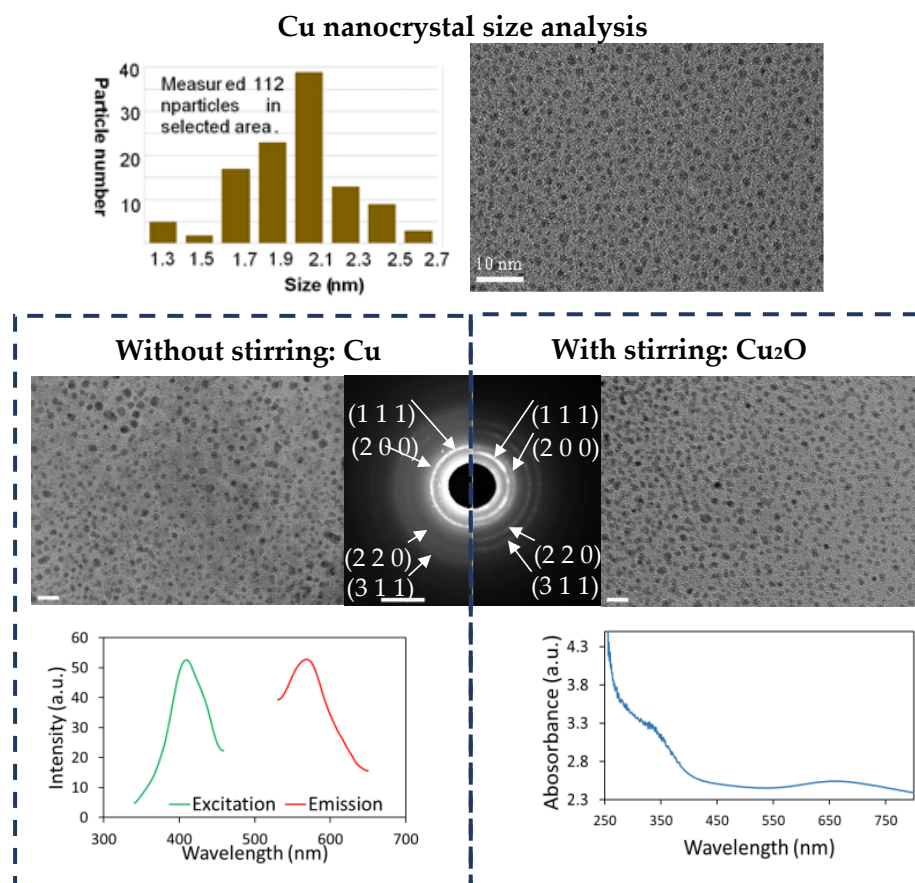


Figure 2. The diffusion process of OH^- ions controls the formation of Cu or Cu_2O nanoparticles. Cu_2O and Cu nanoparticles are produced using an identical synthesis process with and without stirring in the dialysis bag, respectively. Cu nanocrystals have a size about 2 nm and are fluorescent. Cu_2O particles suspension showed its typical UV-Vis absorption spectrum. The scale bars of TEM micrographs and SAED pattern are 10 nm and 5 nm^{-1} , respectively.

3.3. Oxide Nanocrystal Synthesis

When the solution inside the dialysis bag was vigorously stirred in otherwise the same optimized Cu nanoparticle synthesis process, ultrasmall Cu_2O nanoparticles, rather than Cu nanoparticles, were generated (Figure 2) (the mechanism is explained in the Discussion). Using this process, oxide nanoparticles of FeO and CeO_2 were produced (Figures 3 and S6). These extremely small nanoparticles have a size ranging from 1 nm to 3 nm. Citrate cannot reduce these more reactive ions into metal, but for certain ions with multiple valences such as Cu and Fe, the citrate still exhibits the ability to reduce these ions to a lower valence state, as indicated by the reduction of Cu^{2+} to Cu^{1+} and Fe^{3+} to Fe^{2+} . However, for Ce, which is more reactive, Ce^{3+} was oxidized into Ce^{4+} . The chelating effect of citric acid significantly slows down the precipitation reaction of oxide nanoparticles. After the nucleation of the precipitates is triggered, the growth process is so slow that the size range of oxide nanoparticles remains within a few nanometers even after 10 min.

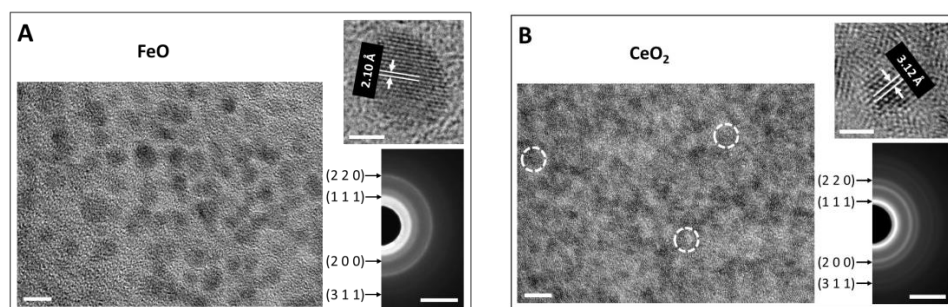


Figure 3. Synthesized ultrasmall oxide nanoparticles. FeO (A) and CeO₂ (B) nanoparticles were synthesized with 1.5 mM FeCl₃ and CeCl₃ salt and 1.5 mM citric acid in the dialysis bag with vigorous stirring, respectively, and 0.5 M NaOH in the reservoir. The scale bars of TEM micrographs corresponding to nanoparticles distribution, lattice fringes, and SAED pattern are 5 nm, 2 nm, and 5 nm⁻¹, respectively.

4. Discussion

The formation mechanisms of these ultrasmall metal nanocrystals are illustrated in Figure 4.

The dialysis membrane forms a diffusion barrier for OH⁻ ions to gradually diffuse from the reservoir into the solution inside the dialysis bag, so that a pH gradient (decreasing from the pH of the NaOH reservoir to the initial pH) is generated in the solution, where different parts of the solution experience a certain pH at different time points, and the solution experiences a gradual pH change from the initial pH (typically about 2) to the pH of the NaOH reservoir.

Citric acid is a weak chelating agent, binding metal ions in solution to form metal chelates. As the pH increases, such chelates become unstable and gradually dissociate to citrate and metal ions. Citrate has long been used as both the mild reductant and stabilizer to synthesize precious metal nanoparticles such as Au, Ag, and Pd, which is referred as the Turkevich method [10–15] and has extensively been investigated [50–54], where metal ions are thought to be reduced by electrons released by oxidation of citrate to 3-oxopentanedioate:

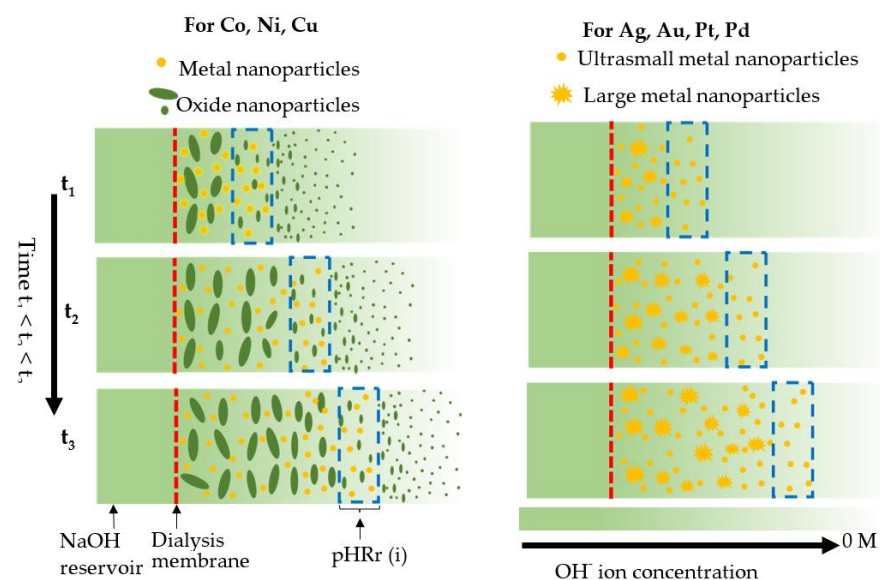
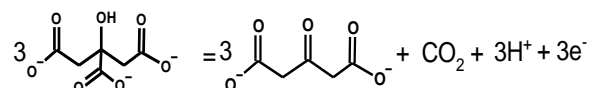


Figure 4. Schematic formation mechanisms of nanocrystals in LDS process. A pH gradient is created in the solution inside the dialysis bag. There exists a pH range, pH_{Rr}(i), in which metal ions are reduced by citrate ions into metal atoms that nucleate and form ultrasmall nanocrystals.

The solution pH can be tuned to control the reduction strength (reduction potential) of citrate; the higher pH, the higher the reduction strength. There exists a pH range for each of these metal ions in which they are reduced by citrate ions into metal atoms that nucleate and form ultrasmall nanocrystals. For convenience of latter discussion, we refer to this pH range as $\text{pHR}_r(i)$ where i represents different metal elements. Even though $\text{pHR}_r(i)$ is unknown, it is guaranteed, as the pH radiates inward, that the solution will sequentially experience $\text{pHR}_r(i)$. When a part of solution experiences pH outside $\text{pHR}_r(i)$, other precipitation reactions or particle formation processes occur. For the cases of Co, Ni, and Cu, when pH is lower than $\text{pHR}_r(i)$ but higher than a certain value, termed as $\text{pH}_0(i)$, citrate is not capable of reducing metal ions into metal atoms, but oxide precipitation reactions can take place to produce oxide nanoparticles. As the pH increases further, passing through $\text{pHR}_r(i)$, the oxide precipitation reaction proceeds at a much higher rate than the citrate reduction reaction, which leads to the formation of large oxide nanoparticles (Figure 2). For Ag, Au, Pd and Pt, when the pH is lower than $\text{pHR}_r(i)$, metal ions are stable, and no reaction occurs. As the pH approaches $\text{pHR}_r(i)$, the citrate reduction reaction takes place. However, if the pH is higher than $\text{pHR}_r(i)$, the citrate reduction reaction rate is too high, which makes nuclei quickly grow into large particles before they are fully capped by citrate ions. Only within $\text{pHR}_r(i)$ can the nucleated ultrasmall nanoparticles be sufficiently capped by citrate ions to prevent them from growing larger. The large particles generated outside $\text{pHR}_r(i)$ can be readily separated from the ultrasmall metal nanocrystals formed in $\text{pHR}_r(i)$ by a simple centrifugation step. The formation of ultrasmall metallic nanoparticles of Co, Ni, Cu, Au, Ag, Pd, and Pt, is accompanied by large particles of Co_3O_4 , NiO, Cu_2O , Au, Ag, Pd, and Pt, respectively (Figure S5).

The formation of Cu_2O rather than Cu nanocrystals when the solution inside the dialysis bag was vigorously stirred in otherwise the same synthesis process (Figure 2) can be well explained by this formation mechanism. Stirring makes the diffusion process proceed at a much higher rate and a pH gradient cannot be established in the solution. This is direct evidence that a pH gradient in the solution is an essential condition to produce metal nanoparticles. Since CuCl_2 was used in the reactant solution, the formation of Cu_2O , instead of CuO, is attributed to the strong reduction capability of citrate ions at high pH.

To further confirm this mechanism, a simple liquid diffusion tube was constructed (Figure 5A). One end of a plastic tube filled with the solution of 1.5 mM CuCl_2 and 1.5 mM citric acid was covered with the dialysis membrane and immersed in the NaOH solution reservoir. It was found that only ultrasmall Cu_2O nanoparticles were generated when 0.05 M NaOH solution was used in the reservoir regardless of the immersion time. The only difference between the tube setup and the dialysis bag setup is the ratio of the surface area of the membrane to the volume of the solution, r , which linearly affects the diffusion rate; the higher the ratio, the higher the reaction rate. r for the dialysis bag setup is much larger than the tube setup (about 15 times higher in our experiments). The result indicates that the synthesis product is also controlled by the diffusion rate of OH^- ions; a relatively high diffusion rate is another necessary condition for generation of metal nanocrystals. Another way to increase the diffusion rate is to use a higher concentration of NaOH solution inside the reservoir. When 0.5 M NaOH solution was used in the reservoir for the tube setup, Cu nanoparticles were indeed generated.

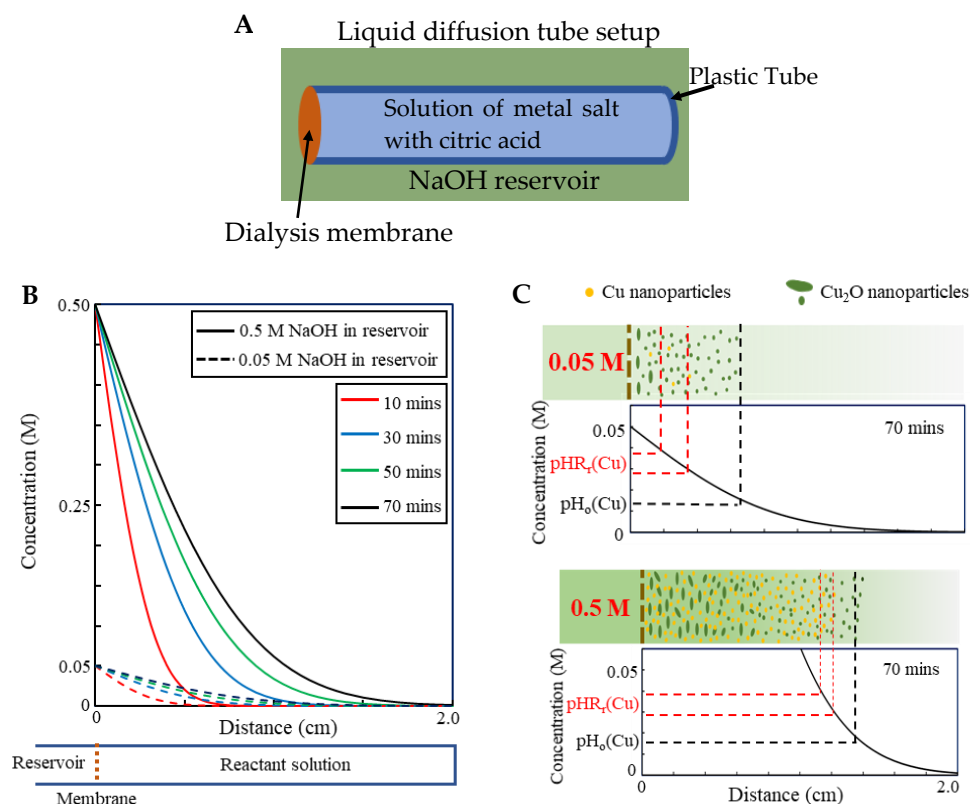


Figure 5. (A) Schematic of liquid diffusion tube. (B) The concentration profile of OH^- in the solution, modeled as the semi-infinite diffusion process with constant surface concentration. (C) The concentration profiles after 70 min for LDS with 0.05 M and 0.5 M NaOH in the reservoir: low concentration of NaOH creates a much more gradual pH gradient which makes large volume of the solution experience a pH below $\text{pHR}_r(\text{Cu})$ for a long time, and therefore, only oxide precipitation reaction takes place and ultrasmall oxide nanoparticles form. High NaOH concentration forms a steep pH gradient which makes $\text{pHR}_r(\text{Cu})$ rapidly sweep through the whole solution volume generating metal nanoparticles.

This diffusion process of OH^- ions at the early stage can be modeled as the semi-infinite diffusion process with constant surface concentration, which has an error function analytical solution to the Fick's second law, with the concentration profile, $C(x, t)$, being expressed as:

$$C(x, t) = C_s - (C_s - C_0) \left[1 - \text{erf} \left(\frac{x}{2\sqrt{Dt}} \right) \right] \quad (1)$$

where x is the distance from the surface, t is the time, C_s the surface concentration, C_0 is the initial concentration in the solution, D is the diffusivity, and erf stands for error function [26]. By taking $C_0 = 0$, and $D = 5 \times 10^{-5} \text{ cm}^2/\text{s}$ [27], the concentration profiles of OH^- ions in the solution from a reservoir containing 0.05 M (C_s) and 0.5 M (C_s) NaOH solution, calculated using Equation (1), are plotted in Figure 5C, respectively. When 0.05 M NaOH solution is used, a gradual pH gradient results in a slower rate of pH change in the solution, so a large volume of the solution experiences a pH below $\text{pHR}_r(\text{Cu})$ but above $\text{pH}_o(\text{Cu})$ for a long time, in which only the oxide precipitation reaction takes place and ultrasmall oxide nanoparticles form. When 0.5 M NaOH solution is used, a steep pH gradient makes $\text{pHR}_r(\text{Cu})$ quickly sweep through the whole solution and the solution experiences a pH below $\text{pHR}_r(\text{Cu})$ for a much shorter period of time, subsequently forming a larger fraction of metal nanoparticles [55].

5. Conclusions

We show that diffusional adjustment of pH in reactant solution can be utilized to produce nanocrystals in a controlled manner. It was found that there exists a pH range for those metal ions in which they are reduced by citrate ions into metal atoms that nucleate and form ultrasmall nanocrystals. Even though such range is unknown, it is guaranteed that the solution will sequentially experience this pH range due to the pH gradient created by the diffusion of hydroxide ions through the dialysis membrane.

Supplementary Materials: The following supporting information can be downloaded at: <https://www.mdpi.com/article/10.3390/cryst14030240/s1>, Figure S1: Schematic of liquid diffusion synthesis steps to produce colloidal Cu nanocrystals title; Figure S2: TEM micrographs and SAED patterns of ultrasmall various nanoparticles with different magnifications; Figure S3: TEM micrographs of Cu nanoparticles produced with different synthesis time; Figure S4: TEM micrographs and SAED patterns of Cu nanoparticles synthesized with various NaOH concentration; Figure S5: TEM micrographs and SAED patterns of large particles formed during the synthesis process; Figure S6: TEM micrographs of oxide nanoparticles with different magnification.

Author Contributions: X.S. and Y.H. (Yaowu Hao) conceived the idea and designed the experiments. S.R.B. and R.H. performed the synthesis and data analysis. J.J. and S.R.B. performed the HRTEM characterizations and analysis. S.R.B. performed magnetic and spectroscopy measurement and analysis. Y.W. aided with diffusion calculation. A.M., S.F., Y.H. (Yi Hong), and Y.C. provided assistance for the synthesis and data analysis. Y.H. (Yaowu Hao) wrote the paper with input from all authors. All authors have read and agreed to the published version of the manuscript.

Funding: This research is supported by the National Institutes of Health (NIH) (R15CA199019 to X.S. and Y.H. (Yaowu Hao)) and the Cancer Prevention and Research Institute of Texas (CPRIT) (PR190678 to X.S. and Y.H. (Yaowu Hao). RP170638 to X.S. and RP110771 to X.S.). Y.H. (Yaowu Hao) and S.F. acknowledge the support from Department of Energy (MSIPP Program, SEEP-IT Consortium). X.S. acknowledges the support from the Dr. Jack Krohmer Professorship funds. Y.H. (Yi Hong) acknowledges the support from National Science Foundation (NSF) (CAREER 1554835). Y.C. acknowledges supports from the Faculty Science and Technology Acquisition and Retention (STARs) Program in the University of Texas System, and the startup funding from the University of Texas at Arlington. Y.H. (Yaowu Hao) acknowledges the Characterization Center for Materials and Biology at UT Arlington.

Data Availability Statement: The original contributions presented in the study are included in the article/supplementary material, further inquiries can be directed to the corresponding authors.

Conflicts of Interest: The authors declare no conflicts of interest.

References

1. Sharapa, D.I.; Doronkin, D.E.; Studt, F.; Grunwaldt, J.D.; Behrens, S. Moving Frontiers in Transition Metal Catalysis: Synthesis, Characterization and Modeling. *Adv. Mater.* **2019**, *31*, 1807381. [[CrossRef](#)]
2. Cargnello, M. Colloidal Nanocrystals as Building Blocks for Well-Defined Heterogeneous Catalysts. *Chem. Mater.* **2019**, *31*, 576–596. [[CrossRef](#)]
3. Jiang, X.Y.; Du, B.J.; Huang, Y.Y.; Zheng, J. Ultrasmall noble metal nanoparticles: Breakthroughs and biomedical implications. *Nano Today* **2018**, *21*, 106–125. [[CrossRef](#)]
4. Bahadori, S.R.; Mulgaonkar, A.; Hart, R.; Wu, C.Y.; Zhang, D.; Pillai, A.; Hao, Y.; Sun, X. Radiolabeling strategies and pharmacokinetic studies for metal based nanotheranostics. *WIREs Nanomed. Nanobiotechnol.* **2020**, *13*, e1671.
5. Liang, M.M.; Yan, X.Y. Nanozymes: From New Concepts, Mechanisms, and Standards to Applications. *Acc. Chem. Res.* **2019**, *52*, 2190–2200. [[CrossRef](#)] [[PubMed](#)]
6. Huang, Y.Y.; Ren, J.S.; Qu, X.G. Nanozymes: Classification, Catalytic Mechanisms, Activity Regulation, and Applications. *Chem. Rev.* **2019**, *119*, 4357–4412. [[CrossRef](#)] [[PubMed](#)]
7. Zhang, Q.; Yang, M.; Zhu, Y.; Mao, C. Metallic nanoclusters for cancer imaging and therapy. *Curr. Med. Chem.* **2018**, *25*, 1379–1396. [[CrossRef](#)] [[PubMed](#)]
8. Chakraborty, S.; Babanova, S.; Rocha, R.C.; Desiredy, A.; Artyushkova, K.; Boncella, A.E.; Atanassov, P.; Martinez, J.S. A hybrid DNA-templated gold nanocluster for enhanced enzymatic reduction of oxygen. *J. Am. Chem. Soc.* **2015**, *137*, 11678–11687. [[CrossRef](#)] [[PubMed](#)]

9. Cushing, B.L.; Kolesnichenko, V.L.; O'Connor, C.J. Recent advances in the liquid-phase syntheses of inorganic nanoparticles. *Chem. Rev.* **2004**, *104*, 3893–3946. [[CrossRef](#)] [[PubMed](#)]
10. Turkevich, J.; Kim, G. Palladium—Preparation and catalytic properties of particles of uniform size. *Science* **1970**, *169*, 873. [[CrossRef](#)]
11. Turkevich, J.; Stevenson, P.C.; Hillier, J. A study of the nucleation and growth processes in the synthesis of colloidal gold. *Discuss. Faraday Soc.* **1951**, *11*, 55–75. [[CrossRef](#)]
12. Ji, X.H.; Song, X.N.; Li, J.; Bai, Y.B.; Yang, W.S.; Peng, X.G. Size control of gold nanocrystals in citrate reduction: The third role of citrate. *J. Am. Chem. Soc.* **2007**, *129*, 13939–13948. [[CrossRef](#)]
13. Piella, J.; Bastus, N.G.; Puntès, V. Size-Controlled Synthesis of Sub-10-nanometer Citrate-Stabilized Gold Nanoparticles and Related Optical Properties. *Chem. Mater.* **2016**, *28*, 1066–1075. [[CrossRef](#)]
14. Bastus, N.G.; Comenge, J.; Puntès, V. Kinetically Controlled Seeded Growth Synthesis of Citrate-Stabilized Gold Nanoparticles of up to 200 nm: Size Focusing versus Ostwald Ripening. *Langmuir* **2011**, *27*, 11098–11105. [[CrossRef](#)] [[PubMed](#)]
15. Bastus, N.G.; Merkoci, F.; Piella, J.; Puntès, V. Synthesis of Highly Monodisperse Citrate-Stabilized Silver Nanoparticles of up to 200 nm: Kinetic Control and Catalytic Properties. *Chem. Mater.* **2014**, *26*, 2836–2846. [[CrossRef](#)]
16. Sun, S.H.; Murray, C.B. Synthesis of monodisperse cobalt nanocrystals and their assembly into magnetic superlattices (invited). *J. Appl. Phys.* **1999**, *85*, 4325–4330. [[CrossRef](#)]
17. van Embden, J.; Chesman, A.S.R.; Jasieniak, J.J. The Heat-Up Synthesis of Colloidal Nanocrystals. *Chem. Mater.* **2015**, *27*, 2246–2285. [[CrossRef](#)]
18. Sun, S.H.; Murray, C.B.; Weller, D.; Folks, L.; Moser, A. Monodisperse FePt nanoparticles and ferromagnetic FePt nanocrystal superlattices. *Science* **2000**, *287*, 1989–1992. [[CrossRef](#)] [[PubMed](#)]
19. Park, J.; An, K.J.; Hwang, Y.S.; Park, J.G.; Noh, H.J.; Kim, J.Y.; Park, J.H.; Hwang, N.M.; Hyeon, T. Ultra-large-scale syntheses of monodisperse nanocrystals. *Nat. Mater.* **2004**, *3*, 891–895. [[CrossRef](#)] [[PubMed](#)]
20. Cargnello, M.; Doan-Nguyen, V.V.T.; Murray, C.B. Engineering uniform nanocrystals: Mechanism of formation and self-assembly into bimetallic nanocrystal superlattices. *Aiche J.* **2016**, *62*, 392–398. [[CrossRef](#)]
21. Liu, S.; Lu, F.; Zhu, J.-J. Highly fluorescent Ag nanoclusters: Microwave-assisted green synthesis and Cr³⁺ sensing. *Chem. Commun.* **2011**, *47*, 2661–2663. [[CrossRef](#)]
22. Suslick, K.S.; Price, G.J. Applications of ultrasound to materials chemistry. *Annu. Rev. Mater. Sci.* **1999**, *29*, 295–326. [[CrossRef](#)]
23. Gedanken, A. Using sonochemistry for the fabrication of nanomaterials. *Ultrason. Sonochem.* **2004**, *11*, 47–55. [[CrossRef](#)] [[PubMed](#)]
24. Rana, R.K.; Mastai, Y.; Gedanken, A. Acoustic cavitation leading to the morphosynthesis of mesoporous silica vesicles. *Adv. Mater.* **2002**, *14*, 1414–1418. [[CrossRef](#)]
25. Peyser, L.A.; Vinson, A.E.; Bartko, A.P.; Dickson, R.M. Photoactivated fluorescence from individual silver nanoclusters. *Science* **2001**, *291*, 103–106. [[CrossRef](#)] [[PubMed](#)]
26. Zhang, J.; Xu, S.; Kumacheva, E. Photogeneration of fluorescent silver nanoclusters in polymer microgels. *Adv. Mater.* **2005**, *17*, 2336–2340. [[CrossRef](#)]
27. Duan, H.; Nie, S. Etching colloidal gold nanocrystals with hyperbranched and multivalent polymers: A new route to fluorescent and water-soluble atomic clusters. *J. Am. Chem. Soc.* **2007**, *129*, 2412–2413. [[CrossRef](#)]
28. Jin, R.; Qian, H.; Wu, Z.; Zhu, Y.; Zhu, M.; Mohanty, A.; Garg, N. Size focusing: A methodology for synthesizing atomically precise gold nanoclusters. *J. Phys. Chem. Lett.* **2010**, *1*, 2903–2910. [[CrossRef](#)]
29. Wilcoxon, J.P.; Provencio, P. Etching and aging effects in nanosize Au clusters investigated using high-resolution size-exclusion chromatography. *J. Phys. Chem. B* **2003**, *107*, 12949–12957. [[CrossRef](#)]
30. Bahadori, S.R.; Dehghani, K.; Bakhshandeh, F. Microstructure, texture and mechanical properties of pure copper processed by ECAP and subsequent cold rolling. *Mater. Sci. Eng. A* **2013**, *583*, 36–42. [[CrossRef](#)]
31. Bahadori, S.R.; Dehghani, K.; Mousavi, S.A. Comparison of microstructure and mechanical properties of pure copper processed by twist extrusion and equal channel angular pressing. *Mater. Lett.* **2015**, *152*, 48–52. [[CrossRef](#)]
32. Mousavi, S.A.; Bahadori, S.R.; Shahab, A. Numerical and experimental studies of the plastic strains distribution using subsequent direct extrusion after three twist extrusion passes. *Mater. Sci. Eng. A* **2010**, *527*, 3967–3974. [[CrossRef](#)]
33. Bahadori, S.R.; Dehghani, K.; Bakhshandeh, F. Microstructural homogenization of ECAPed copper through post-rolling. *Mater. Sci. Eng. A* **2013**, *588*, 260–264. [[CrossRef](#)]
34. Bahadori, S.R.; Mousavi, S.A.; Shahab, A. Sequence effects of twist extrusion and rolling on microstructure and mechanical properties of aluminum alloy 8112. *J. Phys. Conf. Ser.* **2010**, *240*, 012132. [[CrossRef](#)]
35. Zhang, C.; Sun, X.; Li, J.; Liu, Y.-N. Synthesis of Ag nanoclusters by a pH-dependent etching method in aqueous solution. *Nanoscale* **2013**, *5*, 6261–6264. [[CrossRef](#)] [[PubMed](#)]
36. Habeeb Muhammed, M.A.; Verma, P.K.; Pal, S.K.; Retnakumari, A.; Koyakutty, M.; Nair, S.; Pradeep, T. Luminescent quantum clusters of gold in bulk by albumin-induced core etching of nanoparticles: Metal ion sensing, metal-enhanced luminescence, and biolabeling. *Chemistry* **2010**, *16*, 10103–10112. [[CrossRef](#)] [[PubMed](#)]
37. Lin, M.M.; Kim, D.K.; El Haj, A.J.; Dobson, J. Development of Superparamagnetic Iron Oxide Nanoparticles (SPIONS) for Translation to Clinical Applications. *IEEE Trans. Nanobiosci.* **2008**, *7*, 298–305. [[CrossRef](#)]
38. Kansara, K.; Patel, P.; Shukla, R.K. Synthesis of biocompatible iron oxide nanoparticles as a drug delivery vehicle (vol 13, pg 79, 2018). *Int. J. Nanomed.* **2018**, *13*, 4207–4208. [[CrossRef](#)]

39. Wu, W.; He, Q.G.; Jiang, C.Z. Magnetic Iron Oxide Nanoparticles: Synthesis and Surface Functionalization Strategies. *Nanoscale Res. Lett.* **2008**, *3*, 397–415. [[CrossRef](#)]
40. Unsoy, G.; Gunduz, U.; Oprea, O.; Ficai, D.; Sonmez, M.; Radulescu, M.; Alexie, M.; Ficai, A. Magnetite: From Synthesis to Applications. *Curr. Top. Med. Chem.* **2015**, *15*, 1622–1640. [[CrossRef](#)]
41. Takami, S.; Sato, T.; Mousavand, T.; Ohara, S.; Umetsu, M.; Adschiri, T. Hydrothermal synthesis of surface-modified iron oxide nanoparticles. *Mater. Lett.* **2007**, *61*, 4769–4772. [[CrossRef](#)]
42. Wan, L.J.; Yan, S.C.; Wang, X.Y.; Li, Z.S.; Zou, Z.G. Solvothermal synthesis of monodisperse iron oxides with various morphologies and their applications in removal of Cr(VI). *Crystengcomm* **2011**, *13*, 2727–2733. [[CrossRef](#)]
43. Maity, D.; Choo, S.G.; Yi, J.B.; Ding, J.; Xue, J.M. Synthesis of magnetite nanoparticles via a solvent-free thermal decomposition route. *J. Magn. Magn. Mater.* **2009**, *321*, 1256–1259. [[CrossRef](#)]
44. Sun, S.H.; Zeng, H. Size-controlled synthesis of magnetite nanoparticles. *J. Am. Chem. Soc.* **2002**, *124*, 8204–8205. [[CrossRef](#)]
45. Wongwailikhit, K.; Horwongsakul, S. The preparation of iron (III) oxide nanoparticles using W/O microemulsion. *Mater. Lett.* **2011**, *65*, 2820–2822. [[CrossRef](#)]
46. Pandey, S.; Mishra, S.B. Sol-gel derived organic-inorganic hybrid materials: Synthesis, characterizations and applications. *J. Sol-Gel Sci. Technol.* **2011**, *59*, 73–94. [[CrossRef](#)]
47. Hachani, R.; Lowdell, M.; Birchall, M.; Hervault, A.; Mertz, D.; Begin-Coline, S.; Thanh, N.T.K. Polyol synthesis, functionalisation, and biocompatibility studies of superparamagnetic iron oxide nanoparticles as potential MRI contrast agents. *Nanoscale* **2016**, *8*, 3278–3287. [[CrossRef](#)]
48. Sodipo, B.K.; Aziz, A.A. One minute synthesis of amino-silane functionalized superparamagnetic iron oxide nanoparticles by sonochemical method. *Ultrason. Sonochem.* **2018**, *40*, 837–840. [[CrossRef](#)]
49. Osborne, E.A.; Atkins, T.M.; Gilbert, D.A.; Kauzlarich, S.M.; Liu, K.; Louie, A.Y. Rapid microwave-assisted synthesis of dextran-coated iron oxide nanoparticles for magnetic resonance imaging. *Nanotechnology* **2012**, *23*, 215602. [[CrossRef](#)]
50. Gao, Y.H.; Torrente-Murciano, L. Mechanistic insights of the reduction of gold salts in the Turkevich protocol. *Nanoscale* **2020**, *12*, 2740–2751. [[CrossRef](#)]
51. Kimling, J.; Maier, M.; Okenve, B.; Kotaidis, V.; Ballot, H.; Plech, A. Turkevich method for gold nanoparticle synthesis revisited. *J. Phys. Chem. B* **2006**, *110*, 15700–15707. [[CrossRef](#)] [[PubMed](#)]
52. Tyagi, H.; Kushwaha, A.; Kumar, A.; Aslam, M. A Facile pH Controlled Citrate-Based Reduction Method for Gold Nanoparticle Synthesis at Room Temperature. *Nanoscale Res. Lett.* **2016**, *11*, 362. [[CrossRef](#)] [[PubMed](#)]
53. Ojea-Jimenez, I.; Campanera, J.M. Molecular Modeling of the Reduction Mechanism in the Citrate Mediated Synthesis of Gold Nanoparticles. *J. Phys. Chem. C* **2012**, *116*, 23682–23691. [[CrossRef](#)]
54. Agunloye, E.; Panariello, L.; Gavriilidis, A.; Mazzei, L. A model for the formation of gold nanoparticles in the citrate synthesis method. *Chem. Eng. Sci.* **2018**, *191*, 318–331. [[CrossRef](#)]
55. Bahadori, S.R. Synthesis and In Vivo Biomedical Applications of Ultrasmall Metal Nanoparticles. Ph.D. Thesis, University of Texas at Arlington, Arlington, TX, USA, December 2020.

Disclaimer/Publisher’s Note: The statements, opinions and data contained in all publications are solely those of the individual author(s) and contributor(s) and not of MDPI and/or the editor(s). MDPI and/or the editor(s) disclaim responsibility for any injury to people or property resulting from any ideas, methods, instructions or products referred to in the content.